Simulations of twisted bilayer orthorhombic black phosphorus

Douxing Pan,[1,2,3] Tzu-Chiang Wang,[2,*] Wende Xiao,[1] Dongmei Hu,[4] and Yugui Yao[1,†]

[1]*Laboratory of Quantum Functional Material Design and Application, School of Physics,*
Beijing Institute of Technology, Beijing 100081, China
[2]*State Key Laboratory of Nonlinear Mechanics, Institute of Mechanics, Chinese Academy of Sciences, Beijing 100190, China*
[3]*School of Engineering Science, University of the Chinese Academy of Sciences, Beijing 100049, China*
[4]*College of Mechanical Science and Engineering, Jilin University, Changchun 130022, China*

We identified, by means of coincidence site lattice theory, an evaluative stacking phase with a wavelike Moiré pattern, denoted as 2O-tαP, from all potentially twisted bilayer orthorhombic black phosphorus. Such a twisted stacking comes with a low formation energy of -162.8 meV, very close to existing AB stacking, according to first-principles calculations. Particularly, classic molecular dynamic simulations verified that the stacking can be directly obtained in an *in situ* cleavage. The stability of 2O-tαP stacking can be directly attributed to the corrugated configuration of black phosphorus leading to the van der Waals constraining forces, where the top layer can get stuck to the bottom when one layer rotates in plane relative to the other by $\sim$70.5°. Tribological analysis further revealed that the interlayer friction of 2O-tαP stacking reaches up to 1.3 nN, playing a key role in the origin of 2O-tαP.

After the discovery of graphene and development of powerful exfoliation techniques from the well-known scotch-tape method, experimental preparation of two-dimensional (2D) crystals can be expected to perform for any layered van der Waals (vdW) material that is known to chemistry [1–7], such as low-buckled honeycomb silicone and 2D germanium, hexagonal boron nitride (h-BN), and transition-metal dichalcogenides (TMDCs) [3,5,7]. These 2D nanomaterials, displaying similar lattice symmetry, relatively equal lattice parameters, as well as close and high elastic in-plane stiffness, have drawn intense interest from researchers all over the world [2–9], especially for the epitaxial growth, commensurate-incommensurate transition, and thermally induced rotation of graphene on h-BN [5,8,9]. On the tenth anniversary of the birth of graphene, a second fire-new single-element 2D crystal, namely, monolayer orthorhombic black phosphorus, or phosphorene, is emerging as a promising semiconductor with a moderate band gap for nanoelectronics and nanophotonics applications [10–12]. Its few-atomic-layer counterparts give rise to an interesting type of 2D material with many unique properties not found in members of the 2D family [11,12], for instance, significantly anisotropic structure, extremely high hole mobility, strongly linear dichroism, inverse funnel effect, and anomalous accordion effect [7,12–14].

Phosphorene exhibits a corrugated structure with each phosphorus atom covalently bonded with three adjacent atoms belonging to the *Pmna* (or D_{2h}^7) space group (Fig. 1) [7,10,13]. Each atomic layer of phosphorene is coupled by weak vdW forces and stacked in an (AB)^n stacking fashion ($n \rightarrow \infty$), leading to the *Cmca* (or D_{2h}^{18}) space group for the bulk, which dates back to the early years of the last century, when it was obtained by Bridgman successfully via conversion from white phosphorus at high pressure and elevated temperature [12,15]. To date, the monolayer/few-layer phosphorenes have been identified using high-resolution transmission electron

microscope (TEM) and high-angle annular dark-field (HAADF) scanning TEM (STEM) techniques [16,17]. It has been proposed that the physical properties (e.g., band gap, optical response, and exciton binding energy) of bilayer/trilayer/few-layer phosphorenes can be tuned by the stacking orders [18–23], according to first-principles calculations. Five possible stacking orders of bilayer phosphorenes (BP), namely, AA, AB, AC, AD, and Aδ stackings, have been theoretically suggested [18–20], with similar orders for trilayer/few-layer phosphorenes [21–23]. These stackings can be constructed by shifting one phosphorene layer with respect to another, i.e., a shifting stacking fashion. In contrast, a twisted stacking fashion could possess more chances to exist in the real world owing to its multiple alternatives and introduce some novel and intriguing physical properties dating from local symmetry breaking [2,4,5,8,9,24], although they two are of great theoretical significance. Here, by means of coincidence-site lattice (CSL) theory [25], we identified an evaluative twisted BP stacking with twist angle of $\sim$70.5° denoted as 2O-tαP [26]. Such a twisted stacking has a rather low formation energy, very close to the existing AB stacking, according to density functional theoretical (DFT) calculations [27]. Moreover, classic molecular dynamics (MD) simulations [28] verified that the stacking can be directly obtained in an *in situ* cleavage. The stacking conformational and tribological analyses indicated one thing in common: the stability and/or origin of 2O-tαP stacking.

CSL theory. Phosphorene exhibits an underlying 2D Bravais lattice with two orthorhombic basis vectors, $\boldsymbol{a}_1$ and $\boldsymbol{a}_2$, as shown in Fig. 1, which can be expressed as

$$\boldsymbol{a}_1 = a \sin\theta\, \boldsymbol{i}, \quad \boldsymbol{a}_2 = a\cos\theta\, \boldsymbol{j}, \tag{1}$$

where a indicates norm of $(\boldsymbol{a}_1 + \boldsymbol{a}_2)$, θ is incline angle between vectors $\boldsymbol{a}_2$ and $(\boldsymbol{a}_1 + \boldsymbol{a}_2)$, and $\boldsymbol{i}$ and $\boldsymbol{j}$ are unit basis vectors along the horizontal and longitudinal axes, respectively. This Bravais lattice consists of two sublattices, i.e., B (in blue) and A (in green); atoms in B occupy Bravais lattice nodes,

$$\boldsymbol{r}_B(m,n) = m\boldsymbol{a}_1 + n\boldsymbol{a}_2 (m,n \in Z), \tag{2a}$$

*Corresponding author: tcwang@imech.ac.cn
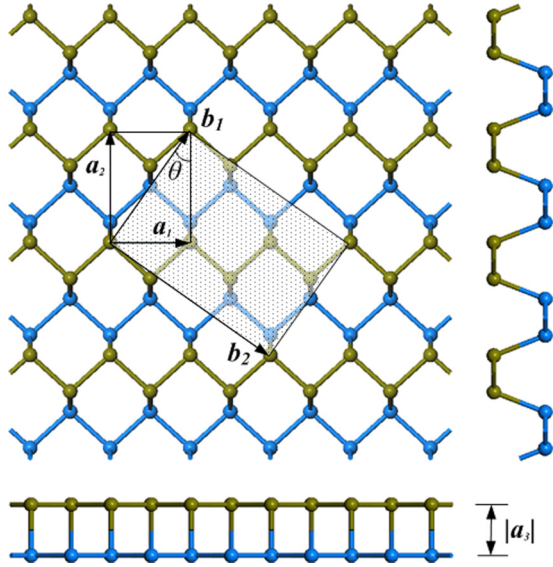†Corresponding author: ygyao@bit.edu.cn

FIG. 1. Lattice structures of monolayer black phosphorus (or phosphorene) in top and side views. Orthorhombic basis vectors $\boldsymbol{a}_1$ and $\boldsymbol{a}_2$ are along the zigzag and armchair directions in the unit cell, respectively, which can generate two supercell lattice vectors, $\boldsymbol{b}_1$ and $\boldsymbol{b}_2$.

and atoms in A are shifted by $\boldsymbol{\Delta} = (\boldsymbol{a}_1 + \boldsymbol{a}_2)/2 + \boldsymbol{a}_3$, i.e.,

$$\boldsymbol{r}_A(m,n) = \boldsymbol{r}_B(m,n) + \boldsymbol{\Delta}(m,n \in Z), \qquad (2b)$$

where $\boldsymbol{a}_3$ is along the out-of-plane direction, the norm of which denotes thickness of the phosphorene, as shown in Fig. 1.

According to CSL theory, a twisted BP layer can be constructed through a relative rotation of the symmetry axes of its two layers, which can be described with a 2D rotation operator R and a rigid translation operator T. Holding the bottom layer fixed, an in-plane rotation of angle φ about the point $\boldsymbol{r}^0$ maps the coordinates $\boldsymbol{r}^1$ in the bottom phosphorene layer into the coordinates $\boldsymbol{r}^2$ in the top one in the manner

$$\boldsymbol{r}^2 = R(\varphi)(\boldsymbol{r}^1 - \boldsymbol{r}^0) + T(t_1,t_2)(t_1,t_2 \in R^*), \qquad (3)$$

and the rigid translation contained in Eq. (3) can be further expressed as

$$T(t_1,t_2) = t_1\boldsymbol{a}_1 + t_2\boldsymbol{a}_2 + h\boldsymbol{a}_3/|\boldsymbol{a}_3|(t_1,t_2 \in R^*), \qquad (4)$$

where h is distance between lamellas of a twisted BP. In some simplified cases, the third term in Eq. (4) is aforethought displaced by h along the out-of-plane direction from the bottom layer to the top so that $T = t_1\boldsymbol{a}_1 + t_2\boldsymbol{a}_2(t_1,t_2 \in R^*)$.

A commensurate operation occurs when a lattice translation of the unrotated phosphorene $\boldsymbol{r}^1$ spanned by its two primitive basis vectors and a similar translation in the rotated one $\boldsymbol{r}^2$ are equal, as illustrated in Fig. 2, where $\boldsymbol{b}_1$ and $\boldsymbol{b}_2$ are two superlattice basis vectors in the twisted BP, both generated by vectors $\boldsymbol{a}_1$ and $\boldsymbol{a}_2$ in Fig. 1. For simplicity, we start with an AA-stacked BP [18] in Fig. 2, the top layer of which is directly vertically displaced from the bottom phosphorene layer by $h = 0.53$ nm [12]. To construct an AB stacking, fix the bottom layer and translate the top layer of the AA stacking horizontally by either $\boldsymbol{a}_1/2$ or $\boldsymbol{a}_2/2$. In the case of pure twisted BP, when the top layer of the AA stacking is rotated in plane
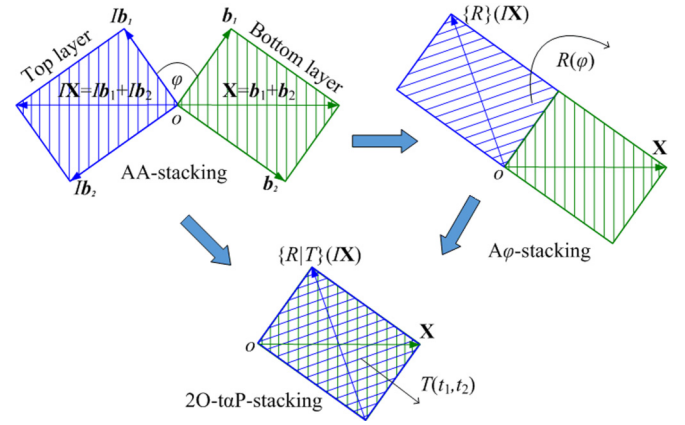

FIG. 2. Forming process of a commensurate twisted bilayer phosphorenes (BP). R indicates a 2D rotation operator, and T a rigid translation operator. $\boldsymbol{b}_1$ and $\boldsymbol{b}_2$ are two superlattice basis vectors in the twisted BP produced. I is an inversion operator commuting with the coordinates $\boldsymbol{X}$ mapped by the superlattice basis vectors.

around the point o relative to the bottom layer without any relative translation, coincidence sites appear at certain angles, and subsequently, twist-type Moiré superstructures emerge. As shown in Fig. 2 for $A\varphi$ stacking, the twist angle φ should satisfy the superlattice coincidence condition

$$\boldsymbol{r}^2(q,p) = R(\varphi)\boldsymbol{r}^1(p,q)(p,q \in Z^*). \qquad (5)$$

According to Eqs. (1) and (2), Eq. (5) occurs only at discrete angles φ that can be indexed by two nonzero integers, p and q (see a detailed derivation in the Supplemental Material [29]), i.e.,

$$\varphi = \arccos\frac{(q^2 + p^2)\cos 2\theta + q^2 - p^2}{q^2 + p^2 + (q^2 - p^2)\cos 2\theta}. \qquad (6)$$

By Eqs. (3), (4), and (6), we can identify a series of twisted stacking BP orders from short- to long-period superlattices, including possible mutually complementary structures (see Table S1 in the Supplemental Material [29]). Especially, for $p = 1$ and $q = 1$, an evaluative stacking with twist angle of $\sim70.5°$ is identified which possesses the smallest period superlattice and is denoted as 2O-tαP stacking [see Figs. 3(a)–3(d) for $t_1 = 2$ and $t_2 = -1$]. The symmetry of 2O-tαP stacking can be described by the $P2_12_12$ (or D_2^3) space group, which is lower than the $Pbcm$ (or D_{2h}^{11}) space group of AB stacking. Compared to the AB stacking, the 2O-tαP stacking exhibits more interesting wavelike Moiré fringes [see Fig. S1 in the Supplemental Material [29] and Fig. 5(b) below].

DFT calculations. To evaluate 2O-tαP stacking, we extracted the unit cell of 2O-tαP stacking and carried out DFT-based first-principles calculations as implemented in the Vienna Ab initio Simulation Package (VASP) [30]. The projector augmented-wave method was used to describe the interactions between ion cores and valence electrons [31]. The unit cell of 2O-tαP stacking was optimized using the exchange and correlation functional of Perdew, Burke, and Ernzerhof (PBE) [32] combined with the DFT-D2 method of Grimme for describing the interlayer vdW forces corrections [33]. An energy convergence criterion of 10^{-4} eV was set for electronic iterations. The geometric structure was fully
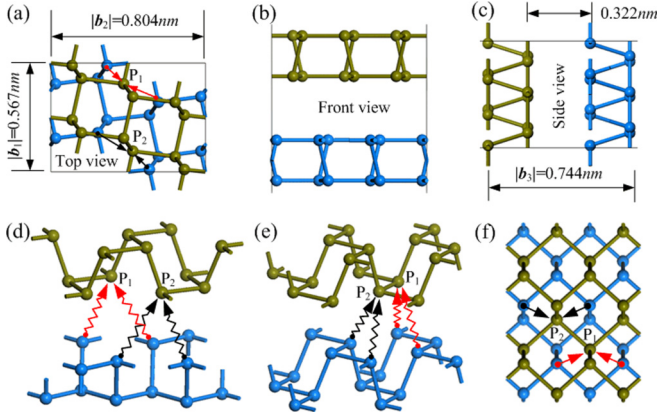
FIG. 3. Superlattice structure of 2O-tαP stacking. Optimized superlattice structure in (a) top, (b) front, and (c) side views, together with unit-cell structural parameters. The interlayer constraining forces of (d) 2O-tαP stacking and (e) AB stacking are denoted by red and black wavy arrows, whose in-plane components are presented in (a) and (f), respectively.

relaxed to allow for the cell volume and shape variations until the Hellmann-Feynman force on each atom was less than 0.01 eV/Å. Kinetic energy for the plane-wave basis set was cut off at 450 eV, which guarantees the absolute energies converge to around 2 meV. The reciprocal space for the unit cell of twisted BP was meshed as $14 \times 10 \times 1$ using the Monkhorst-Pack scheme centered at the Γ point [34]. A vacuum spacing of at least 15 Å was introduced so that the spurious interaction between isolated bilayers can be neglected in the periodic boundary condition. The formation energy per atom is defined as

$$\Delta E_f = (E_2 N_1 - E_1 N_2)/N_1 N_2, \tag{7}$$

where E_1 and E_2 denote total energies of monolayer and bilayer systems of the orthorhombic black phosphorous, respectively; N_1 and N_2 signify numbers of atoms in the unit cell of the single- and double-layered systems, respectively.

The optimized structure of the 2O-tαP-stacking unit cell is presented in Figs. 3(a)–3(d). The relaxed lattice parameters are $|\boldsymbol{b}_1| = 0.567$ nm, $|\boldsymbol{b}_2| = 0.804$ nm, and $|\boldsymbol{b}_3| = 0.744$ nm along three superlattice basis vectors. The area of each unit cell for the 2O-tαP stacking is triple that of its monolayer counterpart [29]. The interlayer distance of 2O-tαP stacking is 0.322 nm, slightly larger than that of the AB stacking [11,21,29], close to the Aδ stacking [23], but much smaller than the AA/AC/AD stackings [18–20,22]. The calculated formation energy is −162.8 meV, slightly larger than that of the AB stacking (−166.8 meV) but significantly smaller than the AA stacking (−153.7 meV). This suggests that the 2O-tαP stacking is an energetically quasistable conformation, which most likely exists in exfoliated bilayer/few-layer black phosphorus. The stability of 2O-tαP stacking can be directly attributed to the corrugated configuration of black phosphorus induced the interlayer vdW constraining forces. It can be seen clearly from Figs. 3(a) and 3(d) that the top layer of 2O-tαP stacking can get stuck to the bottom layer when one phosphorene rotates in plane relative to the other by ∼70.5°. In this case, phosphorus atom P_1 of the top layer undergoes the vdW forces from the two nearest atoms of the bottom
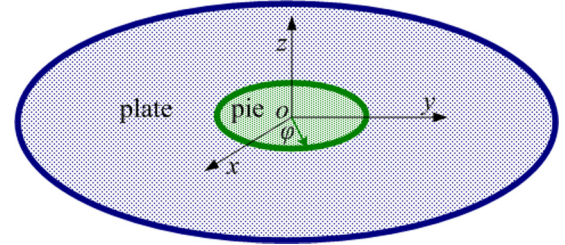

FIG. 4. Computational model with top and front views for a piece of cleavage phosphorene drifting on a black phosphorus substrate surface. The average radii of the pie and plate are 1.73 and 6.32 nm, respectively. The small pie is initially set to be 0.35 nm above the big plate, and the intersection angle between their armchair directions is defined as a twist angle φ.

layer [Fig. 3(d)], so that the in-plane components restrain the displacement of atom P_1 on the top layer [Fig. 3(a)], and so does phosphorus atom P_2, as shown in Figs. 3(a) and 3(d). The existing AB stacking verifies such a stable mechanism in a similar manner, where the top and bottom layers embed in each other right along the armchair and/or zigzag directions. As shown in Figs. 3(e) and 3(f), four symmetrical in-plane components from the interlayer vdW constraining forces of the bottom layer restrict phosphorus atoms P_1 and P_2 of the top phosphorene from shifting on the bottom. As shown by the quantitative tribological analysis in what follows, such vdW interaction-induced interlayer friction of 2O-tαP stacking can reach up to half that of the existing AB stacking.

MD simulations. In an *in situ* cleavage experiment, a piece of phosphorene is usually put on an exposed black phosphorus substrate, which can help verify 2O-tαP stacking. To achieve this goal, we performed classic MD simulations implemented with an open-source software, the Large-scale Atomic/Molecular Massively Parallel Simulator (LAMMPS) code [28]. A subtle drifting model consisting of a small phosphorene pie and big phosphorene plate is established to simulate the *in situ* cleavage, as shown in Fig. 4. For the big one fixed in the reference frame, the in-plane lattice vectors $\boldsymbol{a}_1$ and $\boldsymbol{a}_2$ are along the horizontal (x-axis) and longitudinal (y-axis) directions, respectively. The small pie is initially set to be 0.35 nm above the big plate along the out-of-plane direction (z axis). The intersection angle between the armchair directions of the two phosphorene is defined as a twist angle φ.

In a pure phosphorene system, the interatomic interactions were characterized by the Stillinger-Weber (SW) potential [35]. The SW potential was previously parameterized by Xu *et al.* pretty well, reproducing the crystal structure, cohesive energy, and phonon dispersion predicted by first-principles calculations [36]. Recently, it was applied in the self-assembly of chiral phosphorus nanotubes [37]. The vdW coupling interaction between the ith pie and jth plate phosphorus atoms is depicted by the Lennard-Jones (LJ) potential,

$$V_{LJ}(r) = 4\varepsilon[(\sigma/r)^{12} - (\sigma/r)^6], \tag{8}$$

where $\varepsilon = 0.0132$ eV and $\sigma = 0.3695$ nm for the pie-plate system with a cutoff at 2.1 nm, which were previously applied in calculations of the thermal conductivities of multilayer phosphorenes [38]. The corresponding interlayer friction
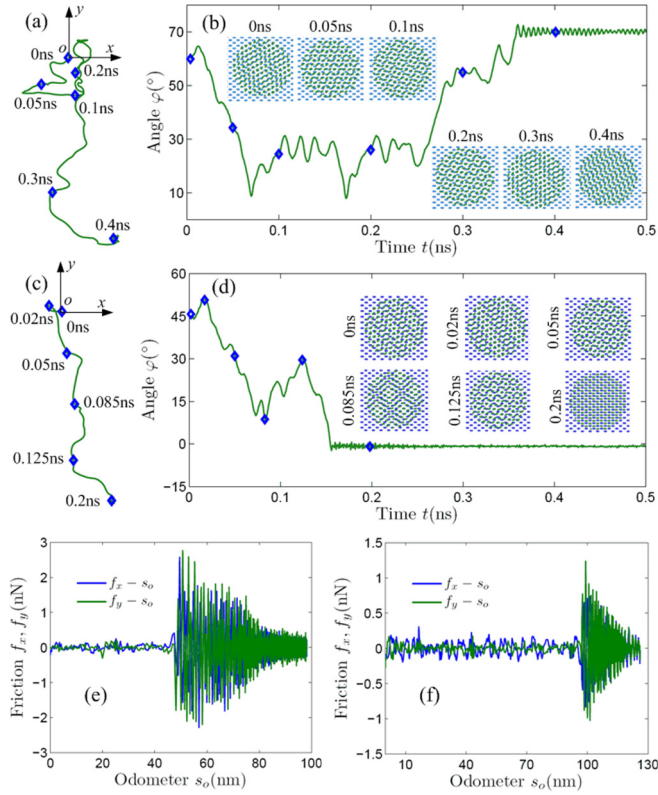
FIG. 5. Thermodynamic features of drifting-induced 2O-tαP/AB settlings at one tenth of room temperature (RT). Drifting trajectories of the mass center for the small pie including six typical moments marked for (a) 2O-tαP stacking with an initial direction of 60° and (c) AB stacking with an initial direction of 45°. Dynamic twist angle as a function of time and six typical Moiré pattern snapshots for (b) 2O-tαP stacking and (d) AB stacking, the times of which are marked in the angle-time curve. The interlayer friction acting on the pie changes with the odometer for (e) AB stacking and (f) 2O-tαP stacking.

acting on the pie can be expressed as

$$\boldsymbol{f} = -\sum_{i=1}^{N_a}\sum_{j=1}^{N_b} \partial V_{LJ}(r_{ij})/\partial \boldsymbol{r}_{ij}, \qquad (9)$$

where i and j denote the ith and jth atoms contained in the pie and plate, respectively; N_a and N_b are numbers of atoms in the pie and plate, respectively; $\boldsymbol{r}_{ij}$ and r_{ij} are the displacement vector and corresponding norm from the nonbonding atom i to j. The odometer of the center of mass (c.m.) for the pie is denoted as s_o, and the in-plane components of the friction along the x and y axes are denoted as f_x and f_y, respectively.

Prior to simulations, the initial equilibrium configurations of the pie and plate were both achieved via the Polak-Ribière conjugate-gradient algorithm [39]. Then the whole pie-plate system under the free boundary condition in three directions was relaxed to reach a stable thermodynamic state using the isothermal-isobaric (NPT) ensemble technique with a time step of 1 fs for ~0.5 ns in one barometric pressure. A Nose-Hoover thermostat at one tenth of room temperature (RT) was used to avoid the pie bursting out of the plate. Figure 5(a) shows the c.m. motion trajectory of the pie. It

is clearly seen that the pie shifts with respect to the plate underneath in search of stable coincidence sites. The twist angle changes with drifting time, as shown in Fig. 5(b). An angle of ~70.5° is stabilized after ~0.36 ns, verifying that the 2O-tαP stacking can be directly obtained in an *in situ* cleavage condition. Six successive snapshots of the rotation motion at 0, 0.05, 0.1, 0.2, 0.3, and 0.4 ns are presented in Fig. 5(b) to evaluate different Moiré superlattices. A video of the comprehensive thermodynamic process is given in the Supplemental Material [29] (2O-tαP-stacking.avi). It is noteworthy that such an interesting thermally induced rotation leading to Moiré superlattices with a specific twist angle has also been observed in recent experiments for graphene on h-BN [9]. For comparison, a drifting trajectory and twist angle-time curve as well as the dynamic process for AB stacking are given in Figs. 5(c) and 5(d) as well as in a movie (AB-stacking.avi) in the Supplemental Material [29]. It can be seen that, besides 2O-tαP stacking and AB stacking, some long-period Moiré superlattices exist that are described by small-angle faults in Table S1 [29]. These superlattices leading to temporary atomic registries, with more exciting Moiré patterns, can be regarded as evolving smoothly [2,4,8].

Figures 5(e) and 5(f) show the interlayer friction acting on the pie changing with the odometer for two types of stackings. Two common features are observed, i.e., stick-slip lubricity [40] at the drifting stage and triangle damping at the settling stage (pinelike friction curve). At the end of the settling stage, the interlayer distances are ~0.310 and ~0.321 nm for AB stacking and 2O-tαP stacking, respectively, in favor of DFT-based calculations. It can be seen from Fig. 5(e) that the interlayer friction can reach up to 2.6 nN for AB stacking. That is why the bulk counterpart of phosphorene is stacked in an $(AB)^n$ stacking fashion ($n \to \infty$). Similarly, a high frictional resistance of 1.3 nN is also observed in Fig. 5(f) for 2O-tαP stacking, almost half that of the existing AB stacking and much higher than the evolving stackings. It constrains the pie from moving to any nonstable/metastable and incommensurate site, playing a decisive role in stabilizing 2O-tαP stacking, directly stemming from the in-plane components of interlayer vdW constraining forces, as discussed above.

To further estimate the distributions of AB stacking and 2O-tαP stacking, a series of drifting-settling simulations was carried out. Three different temperatures were employed below one fifth of RT. For each specific temperature condition, ten different initial directions were considered. The simulation results are presented in Table I.

It can be seen clearly form Table I that the AB stacking dominates at high temperature. Because the pie of AB stacking is stuck in deep potential wells of the plate (the interlayer distance is ~0.310 nm [12,24]) which supply a relatively high interlayer friction [Fig. 5(e)] in comparison to 2O-tαP stacking [Fig. 5(f)] [40,41], the up-down shock activated by high temperature makes the pie jump easily out of the shallow wells for 2O-tαP stacking [41] (the interlayer distance is ~0.321 nm). Conversely, with simulating temperature decreasing, the 2O-tαP stacking has more possibility to settle than the AB stacking. This is mainly due to the corrugated configuration of phosphorene (Figs. 1 and 3). For 2O-tαP stacking, the number of potential shallow wells to sink into is much higher than that for AB stacking, and these shallow wells

TABLE I. Distributions of AB stacking and 2O-tαP stacking and the corresponding drifting-settling times in ten different initial directions at three different simulated temperatures, where φ_0 denotes the initial direction, t drifting time, T the simulated temperature, and φ the twist angle in the settling stage. Drifting times are rounded off to the nearest integer picoseconds that are multiple of five [ref. Figs. 5(b) and 5(d)].

$T = 10$ K (RT/30)			$T = 30$ K (RT/10)			$T = 50$ K (RT/6)		
φ_0	φ	t (ps)	φ_0	φ	t (ps)	φ_0	φ	t (ps)
15°		60	15°		425	30°		510
30°		100	30°		185	54.5°		615
35.5°	70.5° or 109.5°	375	35.5°	70.5°	225	75°	70.5°	170
54.5°		230	60°		355	100°		465
60°		185	75°		250	0°		95
75°		95	0°		80	15°		380
90°		100	45°		150	35.5°		525
0°		50	54.5°	0° or 180°	400	45°	0° or 180°	295
45°	0°	205	90°		550	60°		415
100°		375	100°		290	90°		665

are also found by the pie more easily. Comparing Figs. 5(e) and 5(f), a larger interlayer friction can be found for AB stacking before arriving at the settling stage. To find the AB settling, the pie needs a high acceleration to overcome the frictional resistances nearby; or, to sink into a deep well, the pie needs high thermal energy to climb over the barriers nearby [40,41]. Therefore, Table I further demonstrates that the 2O-tαP stacking can be obtained in an *in situ* cleavage at medium and low temperatures, e.g., a liquid-nitrogen (or at least helium) environment.

In conclusion, we systematically explored all potentially twisted bilayer orthorhombic black phosphorus, where the smallest period superlattice exhibiting an ordered wavelike Moiré pattern, 2O-tαP stacking, was preferentially identified, according to coincidence-site-lattice theory. First-principles calculations showed that the 2O-tαP stacking possesses a low formation energy of -162.8 meV, very close to that of the existing AB stacking. Moreover, the classic molecular dynamics theory based on the Stillinger-Weber potential field verified that the stacking could be directly obtained in an *in situ* cleavage experiment. The stability of 2O-tαP stacking can be directly attributed to the corrugated configuration of black phosphorus leading to the interlayer van der Waals constraining forces, where the top layer can get stuck to the bottom when one layer rotates in plane relative to the other by $\sim$70.5°. Tribological analysis further revealed that the interlayer friction of 2O-tαP stacking even reaches up to half that of the existing AB stacking, playing a conclusive role in the origin of the stacking. The comprehensive application of various techniques and/or analytical methods used for the twisted stacking phases can be, in principle, extended/improved to other van der Waals layered materials, therefore, the study should be helpful to surface/interface physics and nanomechanics issues on semiconductor/optoelectronics devices designs.

[1] K. S. Novoselov, A. K. Geim, S. V. Morozov, D. Jiang, Y. Zhang, S. V. Dubonos, I. V. Grigorieva, and A. A. Firsov, Science **306**, 666 (2004).

[2] S. Shallcross, S. Sharma, E. Kandelaki, and O. A. Pankratov, Phys. Rev. B **81**, 165105 (2010).

[3] C. C. Liu, W. X. Feng, and Y. G. Yao, Phys. Rev. Lett. **107**, 076802 (2011).

[4] E. J. Mele, J. Phys. D **45**, 154004 (2012).

[5] W. Yang, G. R. Chen, Z. W. Shi, C. C. Liu, L. C. Zhang, G. B. Xie, M. Cheng, D. M. Wang, R. Yang, D. X. Shi, K. Watanabe, T. Taniguchi, Y. G. Yao, Y. B. Zhang, and G. Y. Zhang, Nat. Mater. **12**, 792 (2013).

[6] H. Pan, Z. S. Li, C. C. Liu, G. B. Zhu, Z. H. Qiao, and Y. G. Yao, Phys. Rev. Lett. **112**, 106802 (2014).

[7] D. X. Pan, Y. Li, T.-C. Wang, and W. Guo, Acta Mech. Sin. **33**, 71 (2017).

[8] C. R. Woods, L. Britnell, A. Eckmann, R. S. Ma, J. C. Lu, H. M. Guo, X. Lin, G. L. Yu, Y. Cao, and R. V. Gorbachev, Nat. Phys. **10**, 451 (2014).

[9] D. Wang, G. Chen, C. Li, M. Cheng, W. Yang, S. Wu, G. Xie, J. Zhang, J. Zhao, X. Lu, P. Chen, G. Wang, J. Meng, J. Tang, R. Yang, C. He, D. Liu, D. Shi, K. Watanabe, T. Taniguchi, J. Feng, Y. Zhang, and G. Zhang, Phys. Rev. Lett. **116**, 126101 (2016).

[10] A. S. Rodin, A. Carvalho, and A. H. Castro Neto, Phys. Rev. Lett. **112**, 176801 (2014).

[11] L. Li, Y. Yu, G. J. Ye, Q. Ge, X. Ou, H. Wu, D. Feng, X. H. Chen, and Y. Zhang, Nat. Nanotechnol. **9**, 372 (2014).

[12] X. Ling, H. Wang, S. X. Huang, F. N. Xia, and M. S. Dresselhaus, Proc. Natl. Acad. Sci. USA **112**, 4523 (2015).

[13] J. S. Qiao, X. H. Kong, Z.-X. Hu, F. Yang, and W. Ji, Nat. Commun. **5**, 4475 (2014).

[14] P. San-Jose, V. Parente, F. Guinea, R. Roldán, and E. Prada, Phys. Rev. X **6**, 031046 (2016).

[15] P. W. Bridgman, J. Am. Chem. Soc. **36**, 1344 (1914).

[16] P. Yasaei, B. Kumar, T. Foroozan, G. H. Wang, M. Asadi, D. Tuschel, J. E. Indacochea, R. F. Klie, and A. Salehi-Khojin, Adv. Mater. **27**, 1887 (2015).

[17] P. M. Das, G. Danda, A. Cupo, W. M. Parkin, L. B. Liang, N. Kharche, X. Ling, S. X. Huang, M. S. Dresselhaus, V. Meunier, and M. Drndić, ACS Nano **10**, 5687 (2016).

[18] J. Dai and X.-C. Zeng, J. Phys. Chem. Lett. **5**, 1289 (2014).

[19] M. H. Wu, X. F. Qian, and J. Li, Nano Lett. **14**, 5350 (2014).

[20] H. B. Shu, Y. H. Li, X. H. Niu, and J. L. Wang, Phys. Chem. Chem. Phys. **18**, 6085 (2016).

[21] D. Cakir, C. Sevik, and F. M. Peeters, Phys. Rev. B **92**, 165406 (2015).

[22] A. Sengupta, M. Audiffred, T. Heine, and T. A. Niehaus, J. Phys.: Condens. Matter **28**, 075001 (2016).

[23] S. Y. Lei, H. Wang, L. Huang, Y.-Y. Sun, and S. B. Zhang, Nano Lett. **16**, 1317 (2016).

[24] T. Cao, Z. L. Li, D. Y. Qiu, and S. G. Louie, Nano Lett. **16**, 5542 (2016).

[25] W. Bollmann, *Crystal Defects and Crystalline Interfaces* (Springer, Berlin, 1970).

[26] The 1T and 2H as well as 3R phases for transition-metal dichalcogenides, where the digit is indicative of the number of layers in the unit cell and the letter designates the type of symmetry, such as 2H-MoS$_2$ and 3R-WS$_2$, are known [G.-B. Liu, D. Xiao, Y. G. Yao, X. D. Xu, and W. Yao, Chem. Soc. Rev. **44**, 2643 (2015); R. J. Toh, Z. Sofer, J. Luxa, D. Sedmidubský, and M. Pumera, Chem. Commun. **53**, 3054 (2017)]; Due to the Patterson symmetry *Pmmm* of the new stacking belonging to the orthorhombic type exhibited, the name 2O-tαP should be employed, where t means "twisted" and αP is the alternative name of the well-established orthorhombic black phosphorus in the monolayer phosphorus polymorph family [J. Guan, Z. Zhu, and D. Tománek, Phys. Rev. Lett. **113**, 046804 (2014); M. H. Wu, H. H. Fu, L. Zhou, K. L. Yao, and X. C. Zeng, Nano Lett. **15**, 3557 (2015)].

[27] W. Kohn and L. J. Sham, Phys. Rev. **140**, A1133 (1965).

[28] S. Plimpton, J. Comput. Phys. **117**, 1 (1995).

[29] See Supplemental Material at http://link.aps.org/supplemental/10.1103/PhysRevB.96.041411 for the derivation of the twist angle for twisted bilayer phosphorene, auxiliary animations, and complementary references and notes.

[30] G. Kresse and J. Furthmuller, Comput. Mater. Sci. **6**, 15 (1996).

[31] G. Kresse and D. Joubert, Phys. Rev. B **59**, 1758 (1999).

[32] J. P. Perdew, K. Burke, and M. Ernzerhof, Phys. Rev. Lett. **77**, 3865 (1996).

[33] S. Grimme, J. Comput. Chem. **27**, 1787 (2006).

[34] H. J. Monkhorst and J. D. Pack, Phys. Rev. B, **13**, 5188 (1976).

[35] F. H. Stillinger and T. A. Weber, Phys. Rev. B **31**, 5262 (1985).

[36] W. Xu, L. Y. Zhu, Y. Q. Cai, G. Zhang, and B. W. Li, J. Appl. Phys. **117**, 214308 (2015). Besides the SW potential including its modified versions, there are other interatomic potentials which can be also applied to the current case, e.g., OPLS-AA force-field (arXiv:1512.02116), and ReaxFF reactive force-field, http://emnmeeting.org/Asia/computation-and-theory/molecular-dynamics-and-its-applications/.

[37] D. X. Pan, T.-C. Wang, C. Wang, W. Guo, and Y. G. Yao, RSC Adv. **7**, 24647 (2017).

[38] Y.-Y. Zhang, Q.-X. Pei, J.-W. Jiang, N. Wei, and Y.-W. Zhang, Nanoscale **8**, 483 (2016).

[39] L. Grippo and S. Lucidi, Math. Program. **78**, 375 (1997).

[40] E. Gnecco and E. Meyer, *Fundamentals of Friction and Wear on the Nanoscale*, 2nd ed. (Springer, Berlin, 2014).

[41] S. T. Thornton and A. Rex, *Modern Physics for Scientists and Engineers*, 4nd ed. (Cengage Learning, 2013).